

1 Validation of Aura Microwave Limb Sounder BrO observations in the stratosphere

2

3 L.J. Kovalenko<sup>1</sup>, N.L. Livesey<sup>1</sup>, R.J. Salawitch<sup>1</sup>, C. Camy-Peyret<sup>2</sup>, M.P. Chipperfield<sup>3</sup>,

4 R.E. Cofield<sup>1</sup>, M. Dorf<sup>4</sup>, B.J. Drouin<sup>1</sup>, L. Froidevaux<sup>1</sup>, R.A. Fuller<sup>1</sup>, F. Goutail<sup>5</sup>, R.F.

5 Jarnot<sup>1</sup>, K. Jucks<sup>6</sup>, B.W. Knosp<sup>1</sup>, A. Lambert<sup>1</sup>, I.A. MacKenzie<sup>7</sup>, K. Pfeilsticker<sup>4</sup>, J.-P.

6 Pommereau<sup>5</sup>, W.G. Read<sup>1</sup>, M.L. Santee<sup>1</sup>, M.J. Schwartz<sup>1</sup>, W.V. Snyder<sup>1</sup>, R. Stachnik<sup>1</sup>,

7 P.C. Stek<sup>1</sup>, P.A. Wagner<sup>1</sup>, J.W. Waters<sup>1</sup>

8

9

10

11

12 <sup>1</sup>Jet Propulsion Laboratory, California Institute of Technology, Pasadena,

13 California, USA

14 <sup>2</sup>Laboratoire de Physique Moléculaire pour l'Atmosphère et l'Astrophysique,

15 Université Pierre et Marie Curie, Paris, France

16 <sup>3</sup>Institute of Atmospheric Science, School of Earth and Environment, University

17 of Leeds, Leeds, UK

18 <sup>4</sup>Institute of Environmental Physics, University of Heidelberg, Heidelberg,

19 Germany

20 <sup>5</sup>Service d'Aéronomie, Centre National de la Recherche Scientifique, Verrières-

21 le-Buisson, France

22 <sup>6</sup>Harvard-Smithsonian Center for Astrophysics, Cambridge, Massachusetts, USA

23 <sup>7</sup>University of Edinburgh, Edinburgh, UK

24 **Abstract**

25 Validation of stratospheric BrO vertical profiles obtained by the Microwave Limb  
26 Sounder (MLS) on the Aura satellite is discussed. MLS BrO measurements are compared  
27 with expectations of its latitudinal and seasonal dependence, as well as with more  
28 localized balloon-borne measurements of BrO. We describe the expected precision and  
29 systematic errors of the version 2.2 retrieval and show that scientific studies using MLS  
30 BrO vertical profiles require extensive averaging to increase the signal-to-noise ratio to  
31 useful values. A monthly zonal mean over a 10° latitude bin (about 3,000 individual  
32 profiles) results in a precision of  $\sim \pm 4$  pptv ( $\sim 25\%$  of a typical daytime signal).  
33 Moreover, it is necessary to take day/night differences to remove large biases. The  
34 pressure range over which the data are considered useful is 10 to 3.2 hPa. Over this  
35 range, the estimated accuracy in the day/night difference is about  $\pm 20\%$ . The vertical  
36 resolution is 5.5 km for 10 to 3.2 hPa. Day/night differences are a good measure of  
37 daytime BrO from 10 to 4.6 hPa; for 3.2 hPa the non-negligible nighttime BrO needs to  
38 be accounted for. We infer total inorganic bromine ( $\text{Br}_y$ ) to be  $22.1 \pm 5.5$  pptv based on  
39 analysis of MLS measurements of BrO, which implies a contribution of  $6.5 \pm 5.5$  pptv to  
40 stratospheric bromine from sources other than long lived  $\text{CH}_3\text{Br}$  and halons.

41 **1. Introduction**

42 Bromine monoxide (BrO) is an important species in the destruction of stratospheric  
43 ozone, especially in the lower stratosphere [*Salawitch et al.*, 2005; *WMO*, 2003; 2007].  
44 Here we present a validation of stratospheric measurements of BrO by the Microwave  
45 Limb Sounder (MLS) instrument [*Waters et al.*, 2006] on the Aura satellite. This  
46 instrument has been measuring vertical profiles of BrO with global coverage since  
47 August 2004. The latest publicly released version 2.2 data are analyzed here. We discuss  
48 the precision and accuracy of these data, examine how reasonable they are by comparing  
49 with expectations of dependences on latitude and season, and present preliminary  
50 comparisons with balloon-based measurements. Because the abundance of BrO varies  
51 strongly with solar zenith angle and with ambient levels of ozone and nitrogen dioxide,  
52 we also compare total inorganic bromine ( $\text{Br}_y$ ), which is inferred from the BrO  
53 measurements using a photochemical model.

54

55 The Aura MLS BrO data have already been used in a scientific study [*Livesey et al.*,  
56 2006a]. However, that study did not use the version of data available publicly at that  
57 time, v1.5, because v1.5 BrO was determined to be unsuitable for scientific use. Rather,  
58 an interim retrieval version was used, in which a better choice was made in the tradeoff  
59 between precision and vertical resolution. Here we evaluate the latest publicly available  
60 version of BrO retrievals, v2.2, and compare them with the previous version, v1.5, as  
61 well as with the interim version used by *Livesey et al.* [2006a].

62

## 63 2. Description of Aura MLS Observations of BrO

64 The Aura satellite orbits the Earth about 14 times per day. The MLS instrument detects  
65 thermal emission from the Earth's limb in the millimeter- and sub-millimeter-wavelength  
66 ranges as the field of view is scanned vertically through the atmosphere in the plane of  
67 satellite motion. Each vertical scan takes about 24 seconds and consists of 120 different  
68 forward-looking limb radiance measurements, each measurement having an integration  
69 time of about 1/6th of a second. About 3,500 vertical scans are performed each day. At a  
70 given latitude, about half of these measurements are of a sunlit atmosphere (during the  
71 ascending part of the orbit) and half are of a dark atmosphere (the descending part),  
72 except in regions of polar summer or winter, in which case both the ascending and  
73 descending measurements are in daylight (polar summer) or darkness (polar winter). The  
74 local solar time of the MLS measurements is about 1:45 p.m. for the ascending part of the  
75 orbit, and 1:45 a.m. for the descending part, except poleward of about 60° in latitude. The  
76 range of latitudes sampled is from 82°S to 82°N.

77

78 BrO is measured using spectral lines of the  $^{81}\text{BrO}$  isotope that correspond to two  
79 rotational transitions in the vibrational ( $v=0$ ) and electronic ( $J=3/2$ ) ground state,  $N=47/2$   
80  $\rightarrow N'=49/2$ , and  $N=49/2 \rightarrow N'=51/2$ . These transitions, at 624.768 GHz and 650.179  
81 GHz, respectively, are each split into eight lines by  $\Lambda$ -doubling and nuclear quadrupole  
82 effects, and are spread over a range of about 6 MHz. The spectral features are  
83 characterized by *Drouin et al.* [2001], the collision-broadened linewidths are reported by  
84 *Yamada et al.* [2003].

85

86 The MLS BrO signal strength is only about 0.2 K brightness temperature, well below the  
87 individual measurement noise of about 4 K. Thus significant averaging of individual  
88 measurements is required to obtain useful BrO signal-to-noise. The top panel of Figure 1a  
89 shows a typical spectrum of atmospheric emission in the region of the 650 GHz BrO line  
90 as detected by the MLS R4 (640 GHz) radiometer. This spectrum is averaged over one  
91 year of measurements, for latitudes ranging from 55°S to 55°N, at a limb/tangent altitude  
92 of about 40 km. Both daytime measurements (orange) and nighttime measurements  
93 (black) are shown. An interfering ozone line is clearly visible. Taking the difference  
94 between the daytime and nighttime signals, shown in the bottom panel of Figure 1a,  
95 removes the ozone signal, which does not display a diurnal variation at this altitude. The  
96 signal from BrO, which has a strong diurnal variation at this altitude, is thus revealed.  
97 Comparison of the measured spectrum (black) with that predicted from the retrieved  
98 profiles (cyan) shows good agreement. Figure 1b shows similar results for the other BrO  
99 line (at 625 GHz) that is detected by the same radiometer. Both lines are used for the BrO  
100 retrievals.

101

102 The MLS retrieval technique has been described previously [*Livesey et al.*, 2006b].  
103 Profiles are retrieved on a pressure grid of six levels per decade change in pressure (~2.5  
104 km vertical spacing). Retrieved values of BrO are not constrained to be positive because  
105 to obtain a useful signal-to-noise ratio, extensive averaging is required; were the values  
106 constrained to be positive, the average would then be biased positive.

107

108 Data are stored in HDF-EOS version 5 “swath” format, with each file containing data for  
109 a 24 hour period from midnight to midnight universal time. The MLS Version 2.2 data  
110 quality document (a preliminary version available at <http://mls.jpl.nasa.gov/data>) gives  
111 more information on the format and content of these data files. Each MLS retrieved data  
112 value is stored along with a corresponding precision value that quantifies the impact of  
113 MLS radiance measurement noise on the data. As will be discussed below in the section  
114 on precision, the value of the precision is made negative if it is worse than 50% of the  
115 value of the a priori precision. Each profile is classified with three fields indicating the  
116 quality of the data. The “Quality” field indicates how well the measured radiances can be  
117 fit by the retrieval algorithm; higher values indicate a better fit. The “Status” field  
118 contains several flags indicating whether there were enough measured radiances, whether  
119 clouds might have affected the data, and whether there might be other reasons not to use  
120 the data. These Status flags are shown in Table 1. The “Convergence” field indicates how  
121 the radiance fit compares with that expected by the retrieval algorithm. Values near 1.0  
122 indicate good agreement. We recommend only using v2.2 BrO data that meet the  
123 following criteria:

- 124 • Precision value for data point is positive
- 125 • Status field for profile is even
- 126 • Quality for profile is greater than 1.2
- 127 • Convergence for profile is less than 1.6

128

129 Version 2.2 (v2.2) is the 2nd public release of MLS data and has been used to process the  
130 incoming data stream since March 2007. Reprocessing of the data collected since MLS

131 became operational in August 2004 is also in progress using the v2.2 algorithms. These  
132 processing streams have the specific version name v2.21 and include a minor software  
133 patch applied to an earlier version v2.20 that corrects the handling of MLS Level 1  
134 radiances flagged as bad data. We refer to both these versions collectively as  
135 version 2.2 (v2.2). For this validation effort, 93 days of v2.20 data covering late 2004 to  
136 early 2007 were processed with an emphasis on special months or days of interest for  
137 validation (including campaigns).

138

139 Averaging kernels [*Livesey and Read, 2000; Livesey et al., 2006b; Rodgers, 2000*] for the  
140 v2.2 BrO product are shown in Figure 2. They indicate the vertical resolution of the  
141 retrieved product for each pressure level, as well as the dependence of the retrieved  
142 product on the a priori. The dashed black line gives the width of each curve at half  
143 maximum, a measure of the vertical resolution, which for the pressure range of  
144 scientifically useful MLS BrO ranges from ~5.3 km at 10 hPa to ~ 6.0 km at 3.2 hPa.  
145 Values are given in Table 2. The solid black line in Figure 2 is the sum of the averaging  
146 kernel rows for each pressure surface and indicates the relative amount that the retrieval  
147 is based on the MLS measurement as opposed to being based on the a priori; a value near  
148 unity indicates that the retrievals are based almost entirely on the MLS measurement. For  
149 BrO, the profiles are effectively independent of the a priori for pressures of 0.32 hPa and  
150 greater.

151

152 **3. Retrieval**

153 BrO vertical profiles from the first publicly available version, v1.5, are shown in the  
154 upper three panels of Figure 3. The daily zonal mean profiles (black) of the daytime and  
155 nighttime measurements (left-hand and middle panels, respectively) display large  
156 oscillations with altitude, as well as strong biases at low altitude. Taking the average (red)  
157 of these profiles lessens the range of oscillation, while taking the day/night difference  
158 (right-hand panel) lessens the magnitude of the bias. A poor choice of tradeoff between  
159 precision and vertical resolution led to the oscillations, making v1.5 unsuitable for  
160 scientific studies. We then developed a simple interim retrieval version, shown by the  
161 second row of panels in Figure 3, in which a better choice was made in the tradeoff  
162 between precision and vertical resolution. For this interim version, daily zonal mean  
163 radiances were calculated, from which vertical profiles of BrO were then retrieved  
164 [Livesey *et al.*, 2006a]. The most recent version, v2.2, is shown in the bottom three panels  
165 of Figure 3. It differs from v1.5 in that smoother profiles are obtained at the expense of  
166 decreased vertical resolution. Moreover, new ozone spectroscopy is used (*Drouin et al.*,  
167 manuscript in preparation), which significantly reduces v1.5 biases that had been  
168 empirically ascribed to ozone. Figure 3 shows that for the pressure range over which  
169 MLS measurements of BrO are useful, from 10 to 3.2 hPa, (as will be justified below) the  
170 average nighttime v2.2 BrO (red) shows larger positive biases than does the average  
171 nighttime interim version BrO, while the day/night difference is comparable, with v2.2  
172 showing about 3 ppt more BrO than the interim version.

173

#### 174 **4. Precision**

175 The expected precision in each retrieved profile is calculated from radiance noise and  
176 stored in the data files with each retrieval value. As mentioned earlier, as a data quality  
177 flag, the value of the precision is made negative if it is worse than 50% of the value of the  
178 a priori precision. Figure 4 compares the expected precision (thick line) of one  
179 measurement of BrO with the measured precision (circles) based on the scatter in the  
180 retrieved profiles, for both v1.5 and v2.2 retrievals. Also shown is the precision for daily,  
181 monthly, and yearly 10° zonal averages. The precision is seen to have improved in v2.2,  
182 at the expense of vertical resolution. As shown in the figure, a monthly zonal mean over a  
183 10° latitude bin (about 3,000 individual profiles) results in an estimated precision of  
184 about  $\pm 4$  ppt (about 20% of a typical daily signal) over a pressure range from 10 to 3.2  
185 hPa.

186

187 Figure 5 shows a histogram of the distribution of daytime (shaded region) and nighttime  
188 (red line) BrO measurements for four different pressure surfaces over a latitude range  
189 from 55°S to 55°N for the days reprocessed in v2.2 to date. Also shown is a Gaussian fit  
190 (black line) to the daytime measurements, which are seen to have the Gaussian  
191 distribution expected from noise and a width that closely matches the estimated precision.  
192 The diurnal variation in BrO is discernible for the lower altitudes.

193

## 194 **5. Accuracy**

195 We now address quantification of the various sources of systematic uncertainty in the  
196 MLS BrO product. Systematic errors (which are reproducible but cannot be lessened by  
197 averaging) can be introduced into the retrieved product by errors in instrument calibration

198 (e.g., through radiometric calibration and field-of-view characterization), through  
199 spectroscopic uncertainties or approximations, and by approximations in the retrieval  
200 formulation and implementation. A comprehensive assessment of systematic errors and  
201 their effect on all the MLS products can be found in Appendix A of *Read et al.*  
202 [submitted, 2007]. In this section we summarize the results of this assessment relevant for  
203 the BrO product.

204

205 The effect of each identified source of systematic error on MLS measurements of  
206 radiance has been quantified and modeled. These quantified effects correspond to either  
207  $2\sigma$  estimates of uncertainties in each MLS product, or an estimate of the maximum  
208 reasonable uncertainty based on instrument knowledge and/or design requirements. For  
209 each source of systematic error, we have used one of the following two methods to  
210 quantify the effect on the MLS retrieved products.

211

212 In the first method, sets of modeled errors corresponding to the possible magnitude of  
213 each uncertainty have been applied to simulated MLS cloud-free radiances, based on a  
214 model atmosphere, for a whole day of MLS observations. These sets of perturbed  
215 radiances have then been run through the routine MLS data processing algorithms, and  
216 the differences between these runs and the results of an ‘unperturbed’ run have been used  
217 as a measure of the systematic uncertainty in each case. Although the term ‘systematic  
218 uncertainty’ typically refers to an unknown additive bias or scaling factor, many of the  
219 sources of systematic uncertainty in the MLS measurements give rise to additional  
220 ‘scatter’ in the products. For example, although an error in the ozone spectroscopy

221 directly causes a bias on the ozone retrieval, it also has a secondary effect on the retrieval  
222 of other species with overlapping lines. The difference between the retrieved product in  
223 the unperturbed run and the original ‘truth’ model atmosphere is taken as a measure of  
224 uncertainties due to retrieval formulation and numerics. The concentration in the  
225 unperturbed case is plotted against the concentration in the perturbed case. A linear  
226 regression produces an intercept and a slope. The intercept is a measure of errors that are  
227 independent of the concentration (additive bias), while the deviation of the slope from  
228 unity is a measure of errors that are proportional to the concentration (multiplicative  
229 error). When day/night differences are taken, the additive bias errors should cancel, while  
230 the multiplicative errors remain.

231

232 In the second method, the potential impact of some remaining (typically small)  
233 systematic uncertainties has been quantified through calculations based on simplified  
234 models of the MLS measurement system [Read *et al.*, submitted, 2007]. These  
235 calculations provide estimates of possible multiplicative error.

236

237 The left-hand panel in Figure 6 shows an estimate of the potential magnitude of the  
238 additive biases introduced into the v2.2 BrO product by each of the sources of error listed  
239 in the figure. The corresponding panel in Figure 7 zooms in on the pressure region over  
240 which MLS BrO measurements are useful. These values should be considered as  $2\sigma$   
241 estimates of their probable magnitude. The second panel shows additional scatter in the  
242 additive bias introduced by each of these sources.

243

244 The dominant source of additive systematic error in the MLS BrO product is uncertainty  
245 in the MLS radiometric and spectroscopic calibration (cyan), and is mainly due to the  
246 spectral signature introduced in MLS radiances by departures from a linear response  
247 within the signal chain that are not accounted for in the calibration. This uncertainty  
248 alone can cause a potential additive bias in BrO of up to about  $\pm 20$  ppt at 10 hPa, and up  
249 to about  $\pm 100$  ppt at 31.6 hPa. A second major contributor to systematic errors in the  
250 BrO signal is uncertainty in overlapping signals from other species (blue), mainly ozone,  
251 as seen in Figure 1, though nitric acid also contributes. This uncertainty alone can cause a  
252 potential additive bias of up to  $\pm 20$  ppt at 10 hPa, and up to  $\pm 50$  ppt at 31.6 hPa. A third  
253 major contributor to additive bias is pointing (red), which is caused by the impact of  
254 errors in the assumed width of the oxygen line used in the MLS pointing retrieval,  
255 uncertainty in the field of view pointing offsets between the 640 GHz and 240 GHz  
256 radiometers, and the uncertainty in the field of view pointing offsets between the two 118  
257 GHz radiometers and the 240 GHz radiometer. This uncertainty alone contributes up to  
258 about  $\pm 15$  ppt at 10 hPa, and up to  $\pm 50$  ppt at 31.6 hPa.

259

260 The aggregate additive bias uncertainty in MLS BrO measurements, shown by the thin  
261 line in the third panel of Figures 6 and 7, can be as high as about  $\pm 30$  ppt (~400% of the  
262 expected BrO signal) at 10 hPa, decreasing to about  $\pm 6$  ppt (50%) at 3.2 hPa. Because  
263 averages over large numbers of profiles are needed to obtain useful precision for MLS  
264 BrO, the additional scatter (dotted line) introduced into the data from these sources of  
265 uncertainty will become negligible, and thus the aggregate (thick line) of the biases and  
266 scatter will average down to just the biases (thin line).

267

268 The fourth panels in Figures 6 and 7 show the multiplicative uncertainty (the accuracy as  
269 a percent of the signal, as opposed to an additive bias) introduced into the MLS BrO  
270 measurements from the sources of error listed above. For the pressure range over which  
271 MLS BrO measurements are useful, 10 to 3.2 hPa, this scaling uncertainty is up to about  
272  $\pm 20\%$  of the signal.

273

274 We can dramatically reduce the effects of the additive bias in the BrO signal by taking  
275 advantage of the diurnal variation of BrO and subtracting the nighttime signal from the  
276 daytime signal. For pressures of 4.6 hPa and greater, our calculations show that the  
277 nighttime BrO is expected to be negligible, and therefore this difference is a measure of  
278 the daytime BrO. For lower pressures, the subtraction can still be done; however, for the  
279 difference to be a good measure of the daytime BrO, the non-negligible nighttime BrO  
280 signal will need to be taken into account (perhaps with the aid of a photochemical  
281 model). While taking day/night differences minimizes the additive bias, which we treat as  
282 negligible, it does not affect the multiplicative uncertainty factor, which remains at up to  
283 about  $\pm 20\%$ .

284

285 The uncertainty in the MLS BrO data due to systematic errors is summarized in Table 2.  
286 We conclude that it is necessary to take day/night differences in the measurements of  
287 BrO. Even so, because of the extremely large biases at 15 hPa and larger pressures, (+30  
288 pptv at 15 hPa, -40 pptv at 26 hPa, and becoming even more negative for higher  
289 pressures), we conclude that MLS BrO is not useful for scientific studies in this region.

290 For pressures ranging from 10 to 4.6 hPa, and with sufficient averaging, the error analysis  
291 indicates that the MLS BrO abundance uncertainty is about  $\pm 20\%$ . For 3.2 hPa, the  
292 day/night difference can be known to within an uncertainty of 20%, but for this  
293 difference to be a good estimate of daytime BrO, one will need to compensate for the  
294 non-negligible nighttime BrO. We note that this method of taking day/night differences is  
295 not applicable for polar summer and winter, where BrO is constant throughout the day  
296 and night.

297

## 298 **6. Comparison with expectations**

299 The SLIMCAT chemistry-transport model [*Chipperfield, 1999*] was run in ‘near-real  
300 time’ and driven by U.K. Met Office analysis wind and temperature fields. Model results  
301 were sampled at the same locations and times as MLS profile observations. JPL 2002  
302 kinetics [*Sander et al., 2003*] were used, with the addition of the reaction  $\text{BrONO}_2 + \text{O} \rightarrow$   
303  $\text{BrO} + \text{NO}_3$  [*Soller et al., 2001*], which is included in the JPL 2006 kinetics compendium  
304 [*Sander et al., 2006*]. The model was initialized with 16 pptv  $\text{CH}_3\text{Br}$  (long-lived source  
305 for inorganic bromine) plus 6 pptv of  $\text{Br}_y$  (to represent the effect of short-lived sources) at  
306 the 326 K model boundary; model results show that all of the bromine is in the form of  
307 inorganic bromine ( $\text{Br}_y$ ) for pressures less than 30 hPa.

308

309 Figures 8 shows seasonal zonal means of a) ascending, b) descending, and c) the  
310 day/night difference MLS v2.2 BrO as function of pressure and latitude. The precision on  
311 the day/night differences depends on the number of measurement days in that season:  
312 about  $\pm 6$  pptv for SON 2004, DJF 2004/5, and MAM 2005; and about  $\pm 10$  pptv for JJA

313 2005. These plots can be compared with corresponding plots of SLIMCAT BrO, shown  
314 in Figure 9. The MLS BrO day/night difference shows the expected behavior with season  
315 and latitude. At mid-latitudes and tropics, MLS BrO displays a diurnal variation, with  
316 more BrO during the day than at night. In the polar summer and winter regions, with  
317 constant daytime and nighttime, respectively, the MLS day/night difference is close to  
318 zero.

319

320 We take a more quantitative look at the comparison of MLS BrO day/night differences  
321 and SLIMCAT values in the mid-latitude and tropics for the four seasons by using a  
322 scatter plot, shown in Figure 10. As in Figure 9, the MLS data points represent seasonal  
323 zonal means averaged over  $10^\circ$  latitude bins. We see that although the MLS data points  
324 exhibit significant scatter, they are distributed about the SLIMCAT values. Implications  
325 for total inorganic bromine ( $\text{Br}_y$ ) are discussed in Section 8.

326

327 Figure 11 shows vertical profiles of seasonal averages of MLS v2.2 BrO during polar  
328 summer in the northern hemisphere (NH, top panels) and southern hemisphere (SH,  
329 bottom panels), for ascending (daytime) measurements, descending (also daytime)  
330 measurements, and the ascending/descending difference. These are compared with  
331 SLIMCAT model profiles, similarly averaged. Over the pressure range 10 to 3.2 hPa, the  
332 MLS BrO difference profiles are zero within the expected uncertainty. However, for  
333 lower pressures, a large deviation from zero is seen for the SH (lower panel) difference  
334 profile, by as much as  $10 \pm 5$  ppt at 1.5 hPa. Because this difference is not behaving as

335 expected for these lower pressures, we define 3.2 hPa to be the lowest pressure for  
336 scientific use, though this may be overly cautious.

337

338 Figure 12 shows the same as Figure 11 except for polar winter regions. For the NH polar  
339 winter (upper panels), the SLIMCAT model results show that the difference is not  
340 expected to be zero, because over the days included in the seasonal average, there is some  
341 sunlight during the ascending part of the orbit. In this case, the MLS day/night difference  
342 also differs from zero.

343

344 Figure 13 shows a time series of daily zonal mean MLS BrO over the whole mission for  
345 both v1.5 (black) and v2.2 (red) for descending (nighttime) measurements (top panel) and  
346 day/night differences (bottom panel). In the top panel of Figure 13, a discontinuity is seen  
347 in the v1.5 descending (nighttime) data at about March 2006, which was caused by a  
348 change in the spectrometers when MLS band 13 [Waters *et al.*, 2006] was switched off to  
349 conserve measurement capability. It can be seen that this discontinuity is removed by  
350 taking day/night differences, as shown in the bottom panel of Figure 13. As version 2.2  
351 was designed subsequent to the band being switched off, it is reassuring to see that no  
352 corresponding discontinuity is seen in the v2.2 nighttime data.

353

## 354 **7. Comparison with other measurements**

355 We now compare vertical profiles of MLS BrO with measurements by balloon-borne  
356 instruments. While better comparisons would be obtained by taking monthly zonal means  
357 of MLS BrO profiles about the dates and latitudes of each flight, the required v2.2 data

358 are not yet available. Thus, to achieve reasonable precision, we take an average of all 149  
359 days of MLS v2.2 reprocessed to date, over a zonal mean from 55°S to 55°N. This  
360 latitude range is chosen to ensure that measured BrO undergoes a diurnal variation. This  
361 average samples all seasons and a large range of solar zenith angles, 26° to 73°.

362

363 Because BrO abundances vary strongly with solar zenith angle, as well as with local  
364 abundances of O<sub>3</sub> and NO<sub>2</sub>, we also compare vertical profiles of total inorganic bromine  
365 (Br<sub>y</sub>), which are not as sensitive to local conditions. Values of Br<sub>y</sub> are inferred from the  
366 BrO measurements using a photochemical model [*Osterman et al.*, 1997]. Importantly,  
367 since all the organic bromine is expected to have been photochemically converted to  
368 inorganic bromine at altitudes above 25 km, even for cases where the balloon  
369 measurements do not overlap the MLS measurements, the Br<sub>y</sub> comparison is expected to  
370 be meaningful. However, because stratospheric bromine loading has changed over time  
371 [*Dorf et al.*, 2006b; *Montzka et al.*, 2003; *WMO*, 2003], Br<sub>y</sub> depends on the age of air,  
372 which varies with both altitude and latitude. Thus to account for the age of air differences  
373 in the measurements, we also compare them on a plot of Br<sub>y</sub> vs. N<sub>2</sub>O.

374

375 We infer Br<sub>y</sub> vertical profiles from the measured BrO profiles using a Photochemical  
376 Steady State (PSS) box model. The PSS model is constrained to measurements of BrO,  
377 O<sub>3</sub>, and NO<sub>2</sub>, as described in *Sioris et al.* [2006] and *Livesey et al.* [2006a]. Since MLS  
378 does not measure NO<sub>2</sub>, we estimate it from MLS measurements of N<sub>2</sub>O using well-  
379 established tracer relations. We use JPL 2002 kinetics [*Sander et al.*, 2003] with the  
380 addition of the reactions  $\text{BrONO}_2 + \text{O} \rightarrow \text{BrO} + \text{NO}_3$  [*Soller et al.*, 2001], and  $\text{BrO} + \text{OH}$

381  $\rightarrow \text{Br} + \text{HO}_2$  [Bedjanian *et al.*, 2001], both of which are included in JPL 2006 [Sander *et*  
382 *al.*, 2006]. In addition, we update all reaction rate constants for reactions involving  
383 bromine to JPL 06 values. Preliminary runs with JPL 2006 kinetics show that for the  
384 bromine family, model results using JPL 2002 kinetics with these changes are in  
385 agreement with those using JPL 2006 kinetics. The uncertainty in  $\text{Br}_y$  was determined by  
386 performing a sensitivity analysis with the PSS model, individually varying the  
387 abundances of  $\text{BrO}$  and  $\text{NO}_2$ , as well as the rate constants for production and loss of  $\text{BrO}$ ,  
388 and then adding the resulting changes in  $\text{Br}_y$  in quadrature [Sioris *et al.*, 2006].

389

### 390 **7.1 Comparison with DOAS BrO**

391 We first consider measurements of stratospheric  $\text{BrO}$  obtained by the remote-sensing,  
392 balloon-borne, Differential Optical Absorption Spectrometer (DOAS) instrument [Dorf *et*  
393 *al.*, 2006a; Pfeilsticker *et al.*, 2000]. This instrument detects ultraviolet (UV) and visible  
394 light in solar occultation. Figure 14 (left-hand panel) shows a vertical profile of DOAS  
395 measurements of  $\text{BrO}$  (green points) obtained on March 23, 2003 at  $68^\circ\text{N}$  [Dorf *et al.*,  
396 2006a]. This flight sampled air both inside and outside the vortex. The solar zenith angle  
397 (SZA) for these measurements changes with altitude, ranging from  $82^\circ$  to  $88^\circ$ . This  
398 version of the profile was obtained by smoothing the SCDs (Slant Column Densities)  
399 with a Gaussian of full-width-at-half-max (FWHM) of 1km before doing the profile  
400 inversion [Dorf, 2005]. The vertical profile of MLS  $\text{BrO}$  day/night difference is shown by  
401 the black points; the error bars indicate accuracy. Only those MLS data points in the  
402 unshaded region should be compared with the DOAS measurements.

403

404 We note some problems with comparing these DOAS measurements of BrO with the  
405 MLS measurements. First, the DOAS measurements were not obtained in the altitude  
406 region where the MLS BrO day/night difference measurements are suitable for scientific  
407 study (the unshaded region in Figure 14). Second, the high latitude (68°N) sampled by  
408 the DOAS instrument is not included in the average over the MLS measurements, which  
409 covers latitudes ranging from 55°S to 55°N. Third, as the two instruments take  
410 measurements at different solar zenith angles, we would like to use the PSS model to  
411 scale the DOAS BrO, measured at SZA's ranging from 82° to 88°, to the average SZA of  
412 the MLS measurements, about 40°. However, the smallest SZA attained at 68°N in  
413 March is 65°. Thus the dotted green line shows DOAS BrO scaled to a SZA of 65°, the  
414 closest possible to that of MLS BrO. These problems in non-overlapping altitude range,  
415 different SZA's, and different latitudes are overcome by comparing the total inorganic  
416 bromine ( $\text{Br}_y$ ), which is inferred from the measured BrO using the PSS model.

417

418 Figure 14 (right-hand panel) compares  $\text{Br}_y$  inferred by DOAS BrO (green dash), to that  
419 inferred by MLS BrO day/night difference (black dash). While there are no altitudes for  
420 which the DOAS measurements overlap the window of scientifically useful MLS  
421 measurements, at this high up in the stratosphere all the organic bromine should have  
422 been photochemically converted to  $\text{Br}_y$ , and so a comparison of  $\text{Br}_y$  is still relevant. We  
423 see good agreement between the two instruments for inferred  $\text{Br}_y$ ,  $22.1 \pm 4$  ppt for DOAS  
424 when averaged over altitude at and above 25 km, and  $22.1 \pm 5.5$  ppt for MLS when  
425 averaged from 10 to 4.6 hPa. However, since  $\text{Br}_y$  depends on the age of air, which

426 depends on both altitude and latitude, a more meaningful comparison is revealed by  
427 plotting the inferred  $\text{Br}_y$  vs. the tracer  $\text{N}_2\text{O}$ , which will be shown below.

428

## 429 **7.2 Comparison with SAOZ-BrO BrO**

430 Figure 15 (left-hand panel) shows a vertical profile of BrO (blue points) obtained by the  
431 balloon-borne, remote sensing SAOZ-BrO instrument on August 24, 2004 at 52°N.  
432 SAOZ-BrO is also a solar occultation UV/vis spectrometer [Pundt *et al.*, 2002]. For the  
433 SAOZ-BrO measurements, the solar zenith angle ranged from 80° to 90°. The dotted blue  
434 curve is the SAOZ-BrO values scaled to the average SZA (40°) of the MLS  
435 measurements using the PSS model. MLS BrO day/night difference measurements are  
436 shown by the black points, as in Figure 14. Within the window over which the  
437 scientifically useful MLS day/night difference measurements overlap the SAOZ  
438 measurements, the measurements agree within respective uncertainties.

439

440 Figure 15 (right-hand panel) shows  $\text{Br}_y$  inferred by SAOZ-BrO BrO (blue dash), as well  
441 as that inferred by MLS BrO (black dash). MLS-inferred  $\text{Br}_y$  agrees with SAOZ-inferred  
442  $\text{Br}_y$  within the respective uncertainties. It should be kept in mind, however, that because  
443 of the difference in latitude, SAOZ at 52°N while MLS ranging from 55°N to 55°S, the  
444 average age of air will be quite different for the two profiles, and thus a more meaningful  
445 comparison will be shown below when  $\text{Br}_y$  is plotted against  $\text{N}_2\text{O}$ .

446

## 447 **7.3 Comparison with SLS BrO**

448 Figure 16 (left-hand panel) shows a vertical profile of BrO (red points) obtained by the  
449 balloon-borne Sub-millimeter Limb Sounding (SLS-2) instrument on September 20, 2005  
450 at 34°N. This is the first vertical profile of BrO obtained by this instrument, and thus is  
451 somewhat preliminary. SLS-2 is a cryogenic heterodyne instrument that detects  
452 atmospheric emission [Stachnik *et al.*, 1992]. For BrO it detects the 624.768 GHz lines,  
453 corresponding to the <sup>81</sup>BrO isotope, the same lines detected by MLS, though MLS also  
454 uses the 650 GHz lines. The dotted red curve is the SLS-2 BrO scaled to the local time of  
455 the MLS measurements using the PSS model; in this case, since the SLS-2 measurements  
456 are obtained in the daytime (SZA = 51°), the scaling makes almost no change to the  
457 measured profile. In the window over which the useful MLS measurements overlap the  
458 SLS-2 measurements, the SLS BrO agrees with MLS at 10 hPa, but exceeds MLS BrO  
459 by 6 ppt at 4.6 hPa, which is outside the range of uncertainty.

460

461 Figure 16 (right-hand panel) shows Br<sub>y</sub> inferred by SLS-2 BrO (red dashed) and that  
462 inferred by MLS BrO (black dashed). Comparing inferred Br<sub>y</sub>, MLS and SLS-2 agree  
463 within uncertainty. As with the other comparisons, a more meaningful comparison will be  
464 shown below when Br<sub>y</sub> is plotted against N<sub>2</sub>O.

465

#### 466 **7.4 Comparison of Br<sub>y</sub> in tracer space**

467 Figure 17 shows a plot of Br<sub>y</sub> inferred from measurements of BrO by all four instruments  
468 in tracer space (i.e., plotted against N<sub>2</sub>O). The advantage of this plot is that it accounts for  
469 differences in the age of air. For the DOAS curve, the N<sub>2</sub>O was obtained by the Limb  
470 Profile Monitor of the Atmosphere (LPMA) instrument, which flew on the same gondola

471 as DOAS. For the SAOZ curve, the N<sub>2</sub>O is a monthly zonal mean of MLS N<sub>2</sub>O data for  
472 that month for the latitude bin 45°N to 55°N. For the SLS-2 curve, the N<sub>2</sub>O was obtained  
473 by the FIRS-2 instrument [*Chance et al.*, 1996] aboard the same gondola as SLS-2. Also  
474 shown is the ‘expected’ relation (solid cyan) assuming production of Br<sub>y</sub> from only the  
475 known organic precursors CH<sub>3</sub>Br and halons [*WMO*, 2003]. To generate this curve we  
476 took the relation in *Wamsley et al.* [1998] (dashed cyan), which was based on lower-  
477 stratospheric measurements of organic source gases obtained in 1994. We then updated  
478 the curve to the year of stratospheric entry relevant for this comparison, 2000 (solid line),  
479 by scaling the N<sub>2</sub>O and Br<sub>y</sub> to values appropriate for the year 2000 [*WMO*, 2007]. In the  
480 unshaded region of Figure 17, MLS-inferred Br<sub>y</sub> is in agreement with all three of the  
481 other measurements within uncertainty. We also note that in this region, the Br<sub>y</sub> inferred  
482 from all of the instruments exceeds that expected by the organic source gases. We discuss  
483 the implications of this excess Br<sub>y</sub> in the next section.

484

## 485 **8. Summary and Implications**

486 As summarized in Table 2, Aura MLS measurements of BrO using the v2.2 retrieval are  
487 scientifically useful for pressures ranging from 10 hPa to 4.6 hPa, provided day/night  
488 differences are taken to remove biases, and significant averaging is done to reduce  
489 scatter. A maximum pressure of 10 hPa is chosen because large biases are seen in the  
490 nighttime MLS BrO signal. The minimum pressure of 4.6 hPa is chosen because that is  
491 the highest pressure for which day/night differences are a good measure of daytime BrO.  
492 While the useful pressure range can be extended to the 3.2 hPa pressure surface, the  
493 day/night difference will be a good measure of daytime BrO only if the non-negligible

494 nighttime BrO is taken into account, such as by using a photochemical model to compute  
495 the expected diurnal variation. At pressures lower than the 3.2 hPa surface, MLS BrO  
496 data are judged unsuitable for scientific study because the day/night differences in the  
497 summer polar regions do not behave as expected. For a monthly 10° zonal mean, over the  
498 pressure range from 10 to 3.2 hPa, the precision in the day/night difference is  $\pm 4$  ppt and  
499 the uncertainty in the accuracy is about  $\pm 20\%$ . The vertical resolution between 10 and  
500 3.2 hPa is about 5.5 km.

501

502 To compare our current retrieval, v2.2, with the interim retrieval used in a previous study  
503 [Livesey *et al.*, 2006a], we repeat their calculation of total inorganic bromine, Br<sub>y</sub>. In that  
504 study, Br<sub>y</sub> was calculated from the MLS interim-version BrO using the PSS model, and  
505 an annual average was taken over latitudes ranging from 55°S to 55°N and pressures  
506 ranging from 10 hPa to 2.2 hPa. While day/night differences were used over the pressure  
507 range 10 hPa to 4.6 hPa, the ascending measurements were used for the 3.2 and 2.2 hPa  
508 pressure levels. Here we again use the PSS model to calculate Br<sub>y</sub> from MLS BrO, except  
509 we use v2.2 BrO. We take an average over the same latitude range but only over the 149  
510 days of v2.2 retrieved at the time of writing this manuscript. We use only day/night  
511 differences, and average over a smaller pressure range, from 10 hPa to 4.6 hPa, where the  
512 day/night difference is a good measure of daytime BrO. We find a total stratospheric  
513 bromine, Br<sub>y</sub>, of  $22.1 \pm 5.5$  pptv, which is in acceptable agreement with the *Livesey et al.*  
514 value of  $18.6 \pm 5.5$  pptv, within the respective uncertainties of each value.

515

516 As seen in Figure 17, the  $\text{Br}_y$  inferred from MLS measurements of BrO exceeds the  
517 expected value based on the organic precursors  $\text{CH}_3\text{Br}$  and halons. This is in agreement  
518 with mounting evidence that very short-lived source gases (VSLs) are contributing  
519 significantly to the bromine budget [Dorf *et al.*, 2006b; Salawitch *et al.*, 2005; WMO,  
520 2007]. If we use an estimate of 15.6 pptv for the total bromine abundance of the source  
521 gases  $\text{CH}_3\text{Br}$  and halons present in the atmosphere at the time of the MLS measurements  
522 [Livesey *et al.*, 2006a; Montzka *et al.*, 2003], we estimate that the VSLs contribute about  
523  $6.5 \pm 5.5$  pptv to the bromine budget. Moreover, the agreement of MLS day/night  
524 difference BrO with the SLIMCAT model, seen in Figure 10, also supports this  
525 interpretation, since the SLIMCAT model assumed a total inorganic bromine of 22 pptv,  
526 which represents a contribution of 6 pptv from VSLs.

527

528 Our plans for the future include improving the lower-altitude MLS retrievals, where the  
529 vertical distribution of stratospheric bromine is currently a controversial issue. While we  
530 have some understanding as to the sources of large bias in the MLS BrO data for  
531 pressures of 15 hPa and greater, we plan to work on reducing the effect of these sources.  
532 We also plan to examine retrievals of BrO in the polar regions, where for summer and  
533 winter seasons we cannot use day/night differences. It may be possible to characterize the  
534 bias as a function of altitude both for mid-latitudes as well as for the polar regions in the  
535 spring, and then use this result to compensate for the bias in the polar regions during  
536 summer and winter, as was done for MLS ClO in Santee *et al.* [2007]. We do not  
537 understand why the day/night difference for the southern polar summer region did not go  
538 to zero for pressures of 2.2 and less. We plan to further investigate this issue as well.

539

540 **Acknowledgments**

541 Research at the Jet Propulsion Laboratory, California Institute of Technology, is  
542 performed under contract with the National Aeronautics and Space Administration. We  
543 greatly appreciate the efforts of Bojan Bojkov and the Aura Validation Data Center  
544 (AVDC) team, whose work facilitated the MLS validation activities. Thanks to the Aura  
545 Project for their support throughout the years (before and after Aura launch), in particular  
546 M. Schoeberl, A. Douglass (also as co-chair of the Aura validation working group), E.  
547 Hilsenrath, and J. Joiner. We also acknowledge the support from NASA Headquarters, P.  
548 DeCola for MLS and Aura. The SAOZ team thanks M. van Roozendaal (Belgian Institute  
549 for Space Aeronomy) for spectra processing, the Canadian Space Agency (CSA),  
550 Environment Canada, Scientific Instrumentation Limited, the MANTRA PI's K. Strong  
551 and S. Melo (University of Toronto) for flying SAOZ during the MANTRA 2004  
552 campaign, and Centre National d'Etudes Spatiales (CNES) for its financial support.

553 Table 1. Meaning of bits in the 'Status' field.

554

---

Bit	Value <sup>a</sup>	Meaning
0	1	Flag: Do not use this profile (see bits 8-9 for details)
1	2	Flag: This profile is 'suspect' (see bits 4-6 for details)
2	4	Unused
3	8	Unused
4	16	Information: This profile may have been affected by high altitude clouds
5	32	Information: This profile may have been affected by low altitude clouds
6	64	Information: This profile did not use GEOS-5 temperature a priori data
7	128	Unused
8	256	Information: Retrieval diverged or too few radiances available for retrieval
9	512	Information: The task retrieving data for this profile crashed (typically a computer failure)

---

555

556

<sup>a</sup>'Status' field in L2GP file is total of appropriate entries in this column.

557 Table 2. Summary of Aura MLS BrO product<sup>a</sup>  
 558

Region (hPa)	Vertical Resolution (km)	Precision <sup>b</sup> (pptv)	Bias uncertainty <sup>c</sup> (pptv)	Scaling uncertainty <sup>c</sup> (%)	Comments
2.2 and less	-----	-----	-----	-----	Unsuitable for scientific use
3.2	6	± 5	± 6	± 20	Need to account for non-negligible nighttime BrO
4.6	5.5	± 4	± 9	± 20	
6.8	5.5	± 4	± 20	± 20	
10	5.5	± 4	± 30	± 20	
150 - 15	-----	-----	-----	-----	Unsuitable for scientific use
1000 - 215	-----	-----	-----	-----	Not retrieved

559  
 560 <sup>a</sup> Because of large biases in the data, the daytime and nighttime BrO data at all pressure levels are  
 561 unsuitable for scientific use. Rather, day/night differences must be used. Note that day/night differences are  
 562 not useful for polar winter and summer, where BrO does not undergo a diurnal variation.

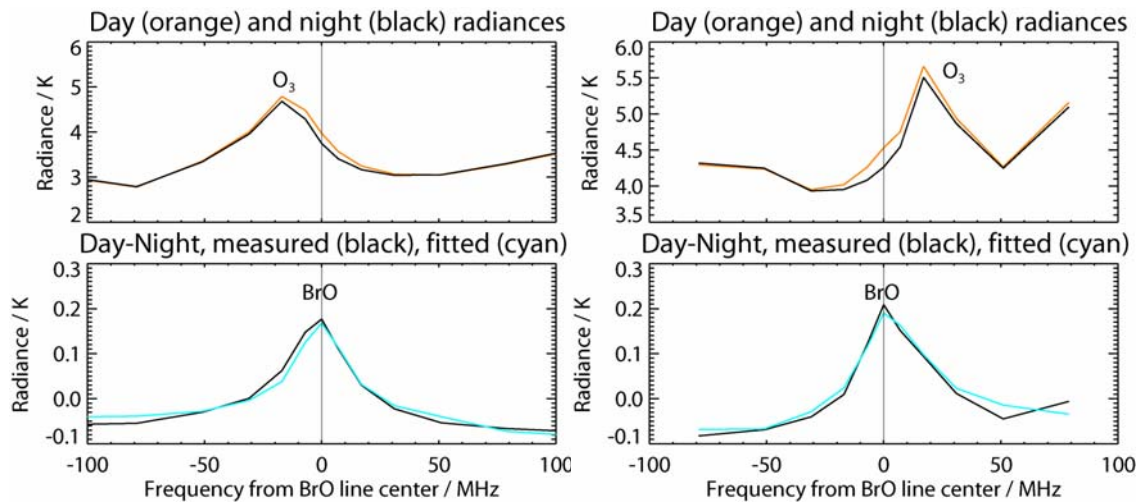
563 <sup>b</sup> Precision is for a 10° monthly zonal mean profile

564 <sup>c</sup> Accuracy is based on the systematic error tests

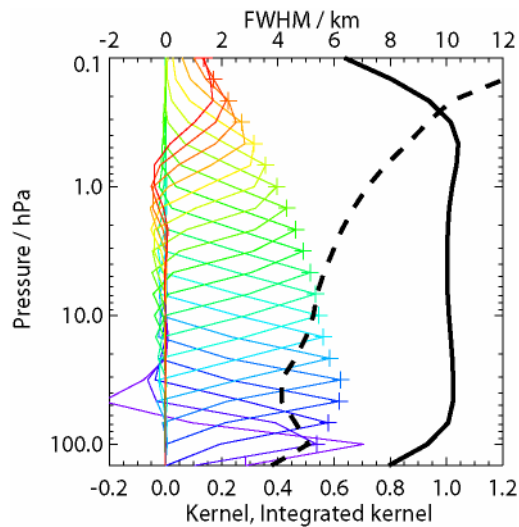
565 Figure 1 a) Radiance spectrum of atmospheric emission in the region of the 650 GHz  
 566 BrO line, MLS spectral band B11F, as detected by the R4 (640 GHz) radiometer, at an  
 567 altitude of 40 km. The spectrum is averaged over one year, over latitudes ranging from  
 568 55°S to 55°N, and from 10 to 2.2 hPa.. b) Same as in a) except for the 625 GHz BrO line,  
 569 MLS spectral band B31M. Upper panels show both the daytime (orange) and nighttime  
 570 (black) radiances, revealing an overlapping ozone line. Lower panels show the difference  
 571 between the day and night signals (black), revealing the BrO line. The cyan line is the  
 572 spectrum predicted from the measured profiles.  
 573

574 a) 650 GHz (B11F spectral band)

b) 625 GHz (B31M spectral band)

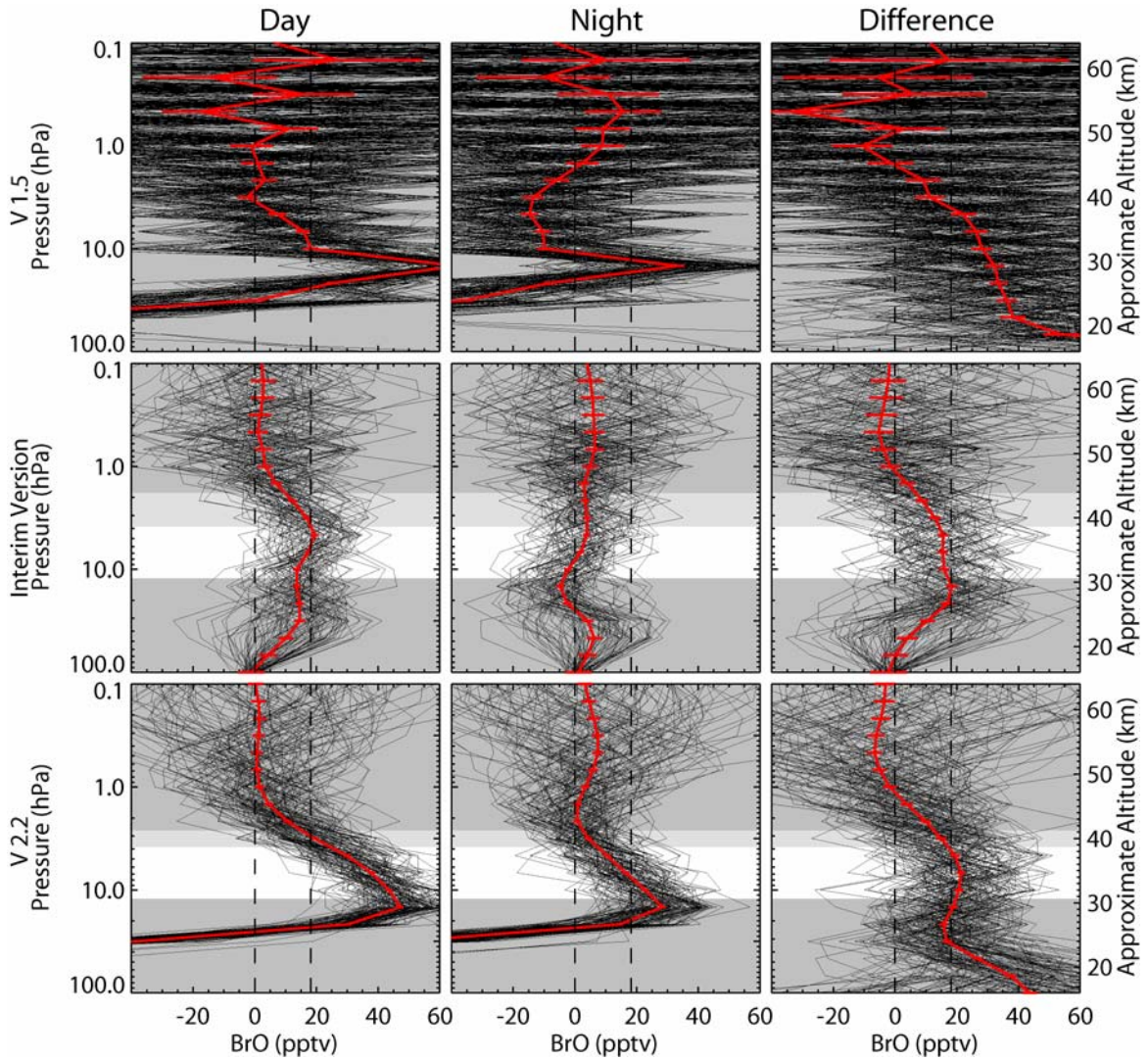


575 Figure 2 Vertical averaging kernels (integrated in the horizontal dimension for five along-  
 576 track profiles) for MLS v2.2 BrO at a latitude of 35°N. Variation in the averaging kernels  
 577 is sufficiently small that these are representative of all profiles. Each colored curve shows  
 578 the averaging kernel for a particular MLS pressure surface (denoted by a plus sign in the  
 579 corresponding color) and indicates the region of the atmosphere from which information  
 580 is contributing to the measurements on that individual retrieval surface. The full-width at  
 581 half maximum (FWHM) of each curve along the pressure axis is a measure of the vertical  
 582 resolution of the retrieved profile for that pressure surface. That width, as measured in km  
 583 (top axis), is shown by the dashed black curve. The solid black curve shows the sum of  
 584 the averaging kernel columns for each of the pressure surfaces (i.e., is the integrated area  
 585 under each 2-dimensional kernel, both horizontal and vertical) and is an indication of  
 586 how much of the retrieved product is based on the a priori. Values near unity imply that  
 587 the majority of information for that MLS data point has come from the measurements,  
 588 while values near zero imply the majority has come from the a priori.

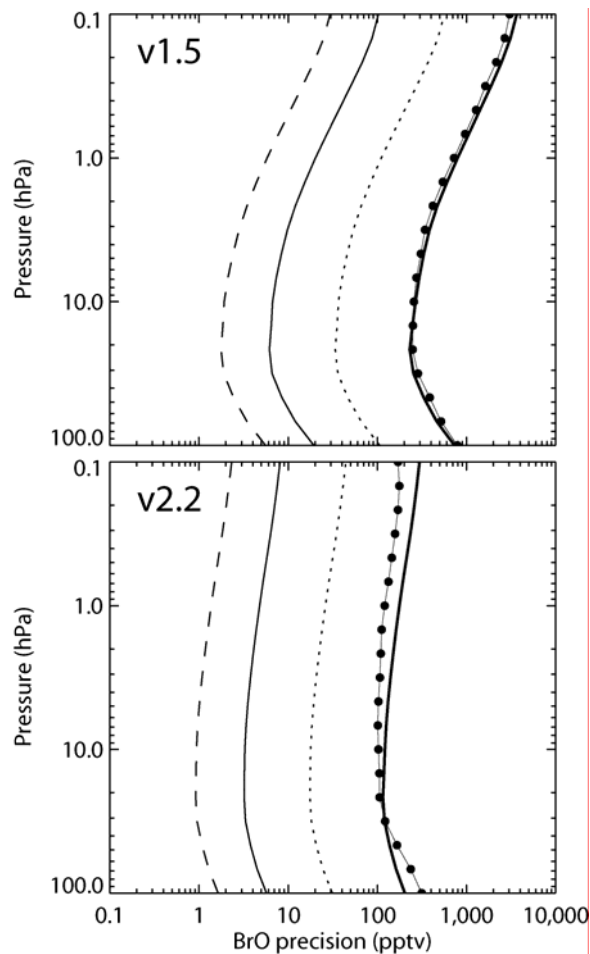


589  
590  
591  
592  
593  
594  
595  
596  
597  
598  
599  
600  
601

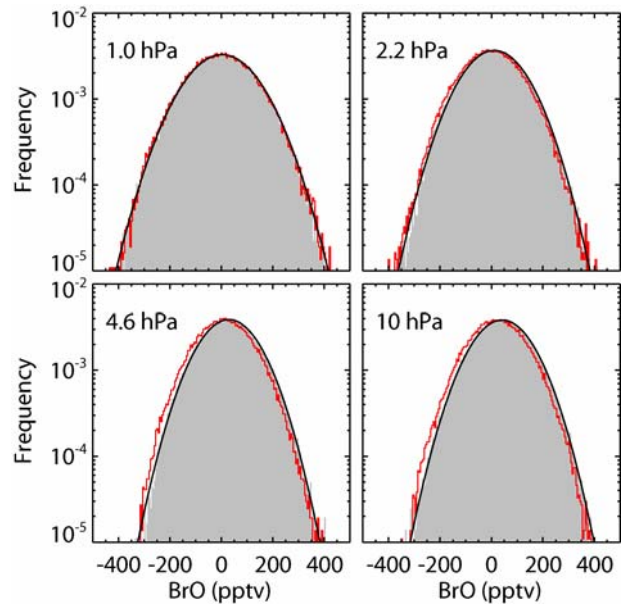
Figure 3 Vertical profiles for three retrieval approaches for daytime, nighttime, and day/night difference. Profiles are averaged over all 149 days retrieved for v2.2 to date and over latitudes from 35°N to 45°N. Top panel shows version 1.5, middle panel the interim version, and bottom panel version 2.2. Black profiles are daily zonal means; red is the average. Error bars show precision only. (We note that the average for the interim version corresponds to the version 2.2 subset of retrieved days occurring before March 5, 2006; after this date, data for the interim version were not processed.) To make comparison easier, a dashed vertical line is drawn at 18.2 ppt, the value of the interim version average BrO at 10 hPa. Regions shaded dark gray indicate where MLS BrO has been determined to be unsuitable for scientific use. Regions shaded light gray indicate where nighttime BrO needs to be taken into account in the day/night difference for that difference to be a good measure of daytime BrO.



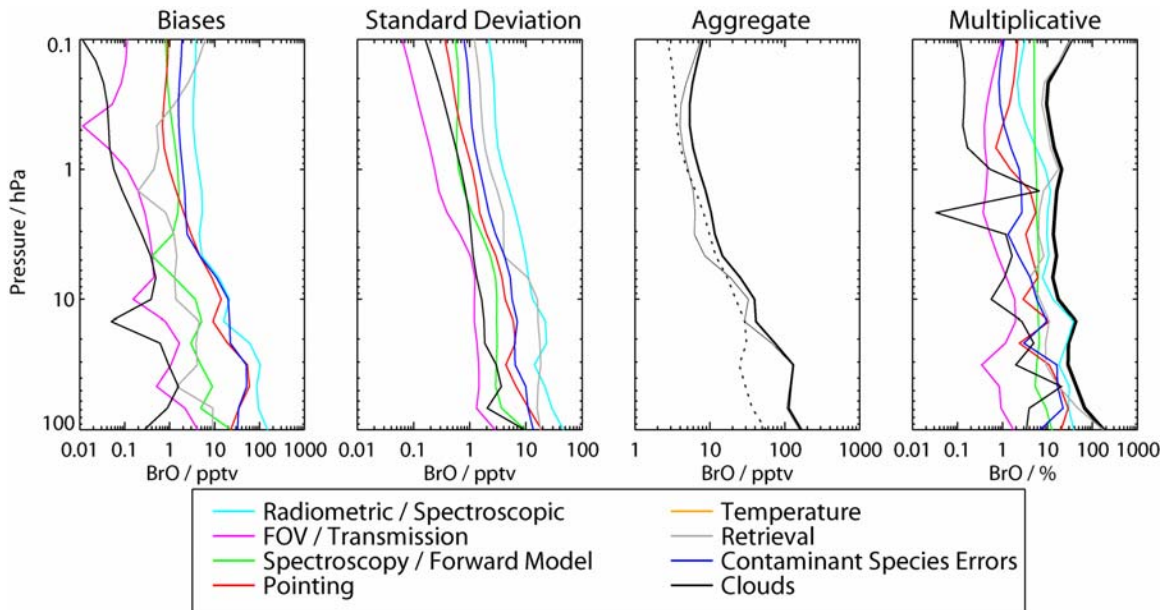
602 Figure 4 Comparison of the measured precision (circles) with that expected from the  
603 retrieval (thick solid line), for a single profile, for v1.5 (upper panel) and v2.2 (lower  
604 panel). The measured precision on a single profile was determined from the scatter in  
605 nighttime profiles retrieved over one day within a 10° latitude bin. Also shown is the  
606 expected precision for the day/night difference of 10° zonal mean profiles averaged over  
607 a day (dotted line), a month (thin solid line) and a year (dashed line).



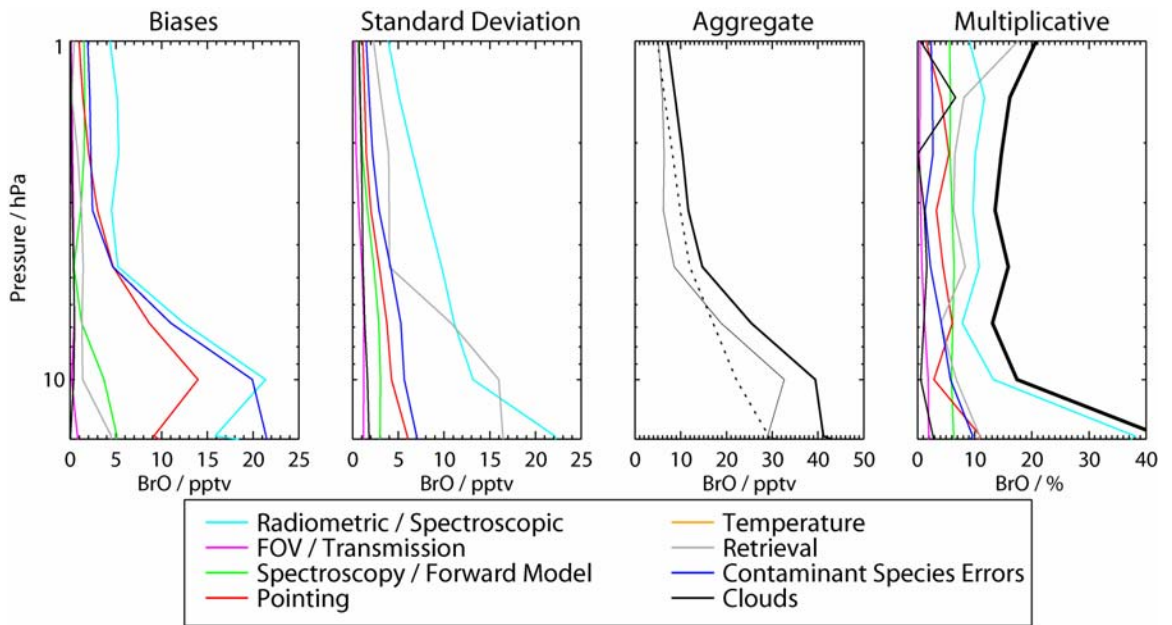
608 Figure 5 Histogram showing the distribution of daytime (shaded region) and  
609 nighttime (red curve) MLS BrO measurements at four different pressure surfaces for  
610 a latitude range from 55°S to 55°N for all the v2.2 data processed to date. The black  
611 line shows a Gaussian fit to the daytime data.



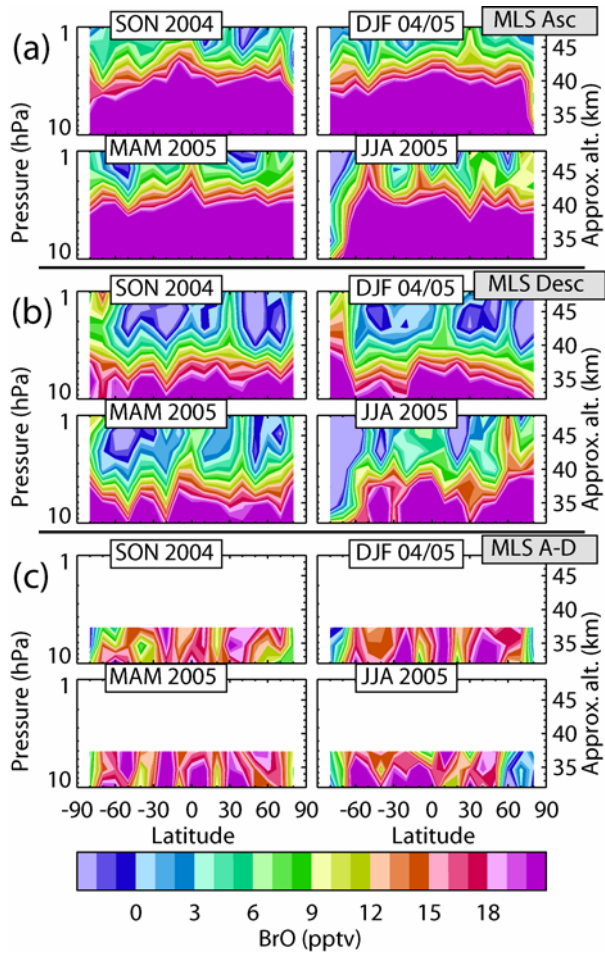
612 Figure 6 Estimated accuracy in v2.2 BrO measurements. The left-hand panel shows the  
 613 estimated potential magnitude of the systematic additive error, or bias, introduced into  
 614 BrO by each of eight sources, while the second panel shows the additional scatter (see  
 615 text) introduced into the retrieved values by each of the sources of uncertainty. The third  
 616 panel shows the root sum squares (RSS) of all the biases (thin solid); the RSS of all the  
 617 additional scatters, or standard deviations (dotted); and the RSS of the two (thick solid).  
 618 The right-hand panel shows the estimated potential multiplicative bias.



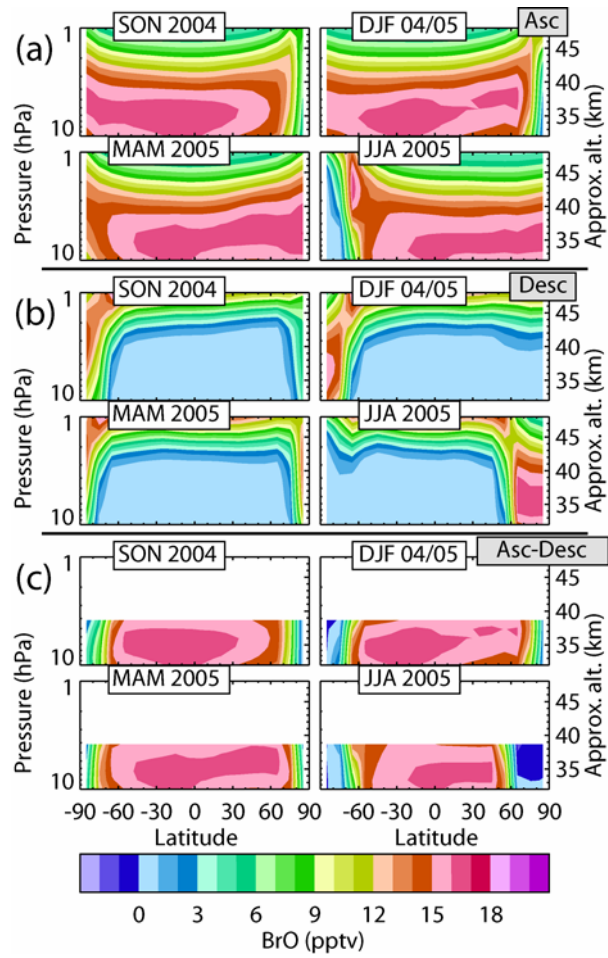
619 Figure 7 Same as Figure 6 except that it is a blowup of the pressure region over which  
 620 MLS BrO is scientifically useful. Note that the x-axis is linear.



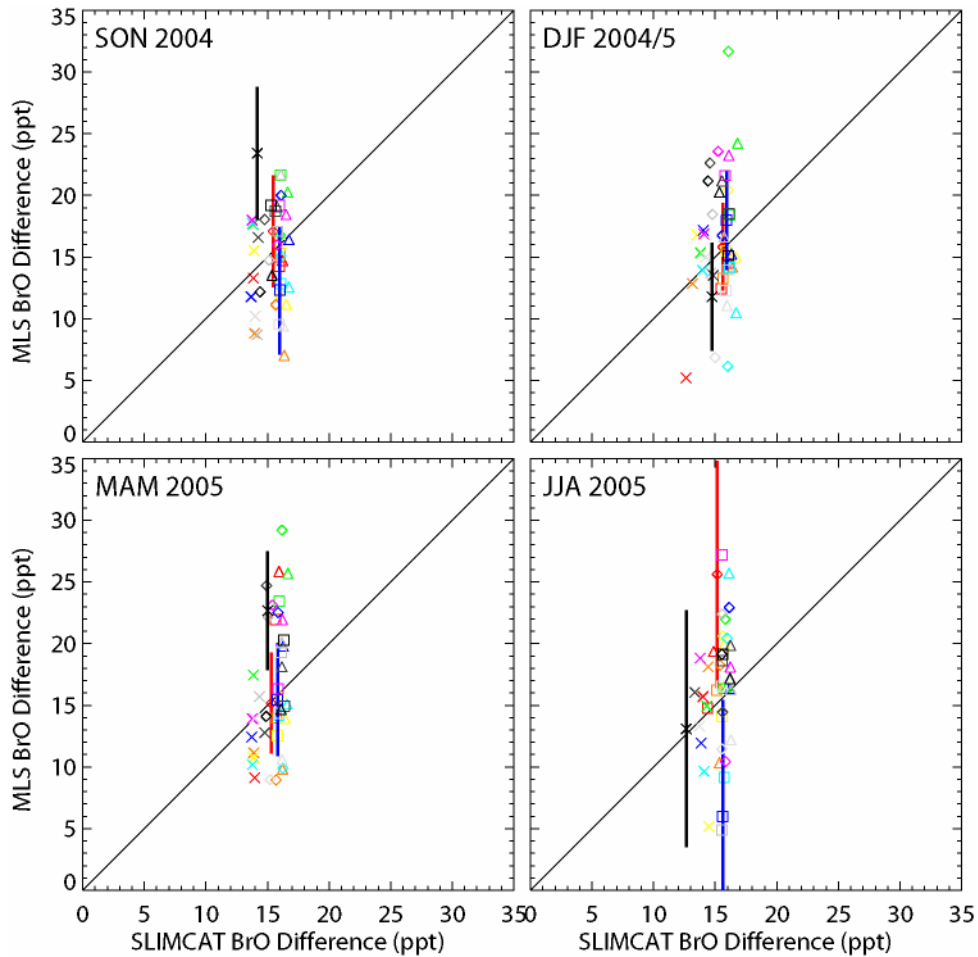
621 Figure 8 Seasonal zonal means of MLS BrO observations for a) ascending (mainly  
 622 daytime) and b) descending (mainly nighttime) phases of the orbits. c) To alleviate biases  
 623 in the lower altitude regions, the ascending/descending difference can be used as a  
 624 measure of daytime BrO, so long as the expected nighttime abundance of BrO is  
 625 negligible, which is the case for MLS difference data on the 4.6 hPa and greater pressure  
 626 surfaces shown here.



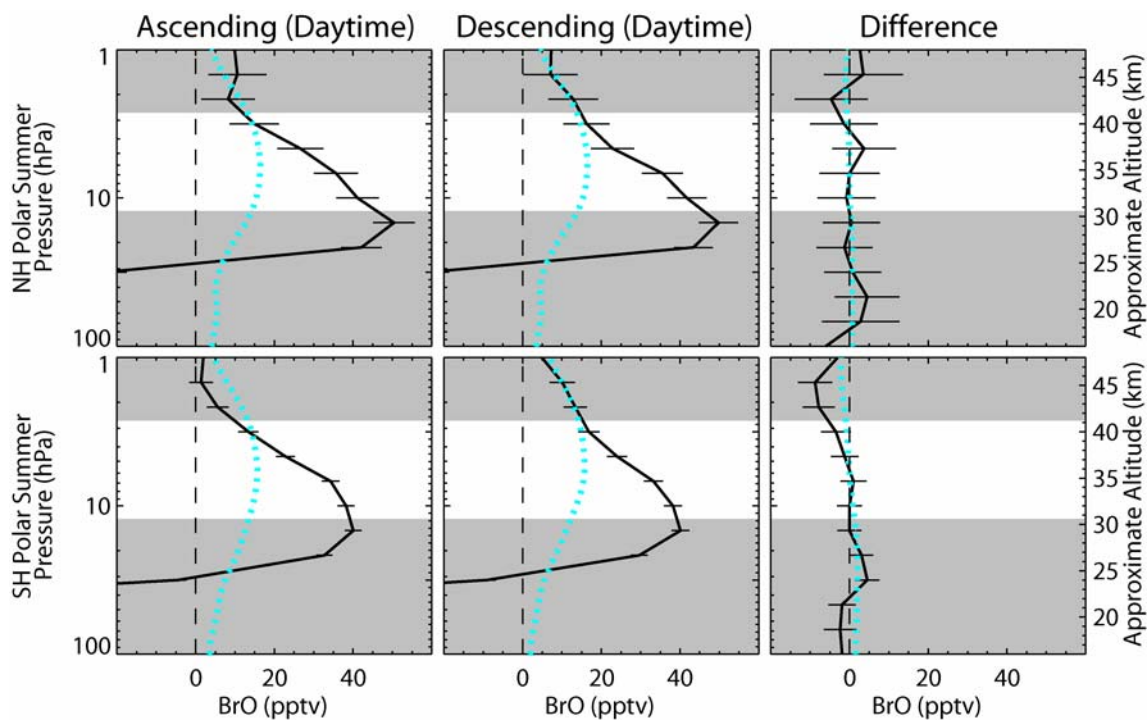
627 Figure 9 Same as Figure 8 except for SLIMCAT.



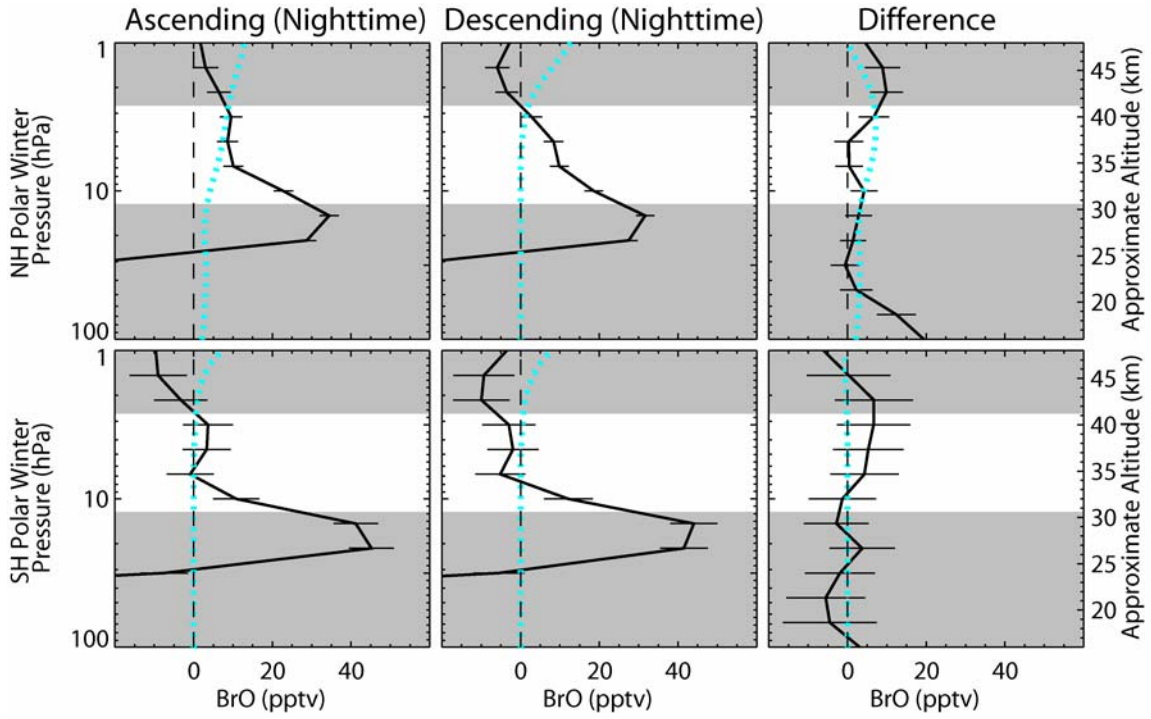
628 Figure 10 Scatter plot of mid-latitude and tropics MLS day/night difference BrO data  
 629 versus SLIMCAT. Data points represent seasonal 10° zonal means, as in Figure 9c, for  
 630 pressures ranging from 10 to 3.2 hPa. Different symbols represent the four pressure  
 631 surfaces, different colors represent the 11 latitude bins. The MLS error bars show the  
 632 scatter (1σ standard deviation) of the daily zonal means about the seasonal average for  
 633 three representative latitudes and pressures.



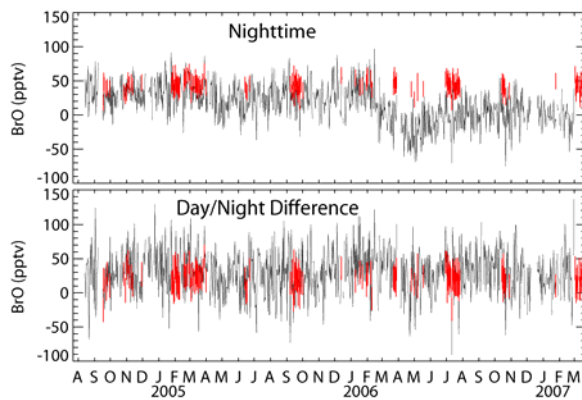
634 Figure 11 MLS v2.2 BrO vertical profiles for polar summer for ascending (daytime)  
 635 measurements, descending (also daytime) measurements, and ascending/descending  
 636 differences (which are expected to be zero). The profiles are seasonal averages of daily  
 637 zonal means; the error bars show the precision. Upper panels shows the NH mean for  
 638 four days in June, July, and August 2005 in the latitude range 75°N to 82°N, while the  
 639 lower panel shows the SH zonal mean for 22 days in December, January, and February  
 640 2004-5 in the latitude range 75°S to 82°S. Regions shaded with dark gray indicate where  
 641 MLS BrO has been determined to be unsuitable for scientific use. Also shown are  
 642 corresponding SLIMCAT model profiles (cyan).



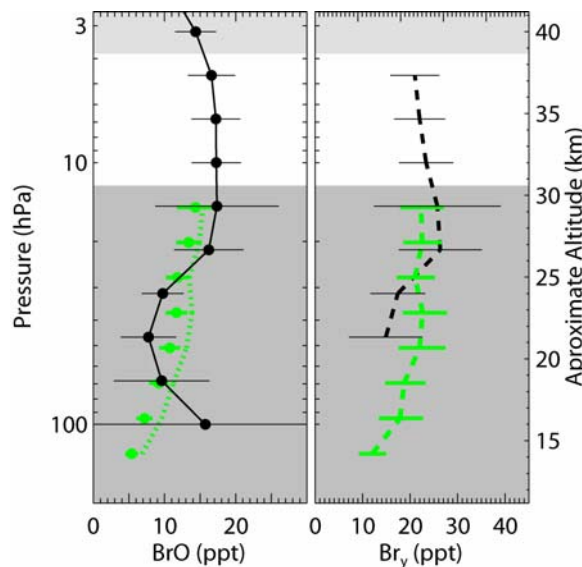
643 Figure 12 Same as Figure 11 except for polar winter. Regions shaded with dark gray  
644 indicate where MLS BrO has been determined to be unsuitable for scientific use.



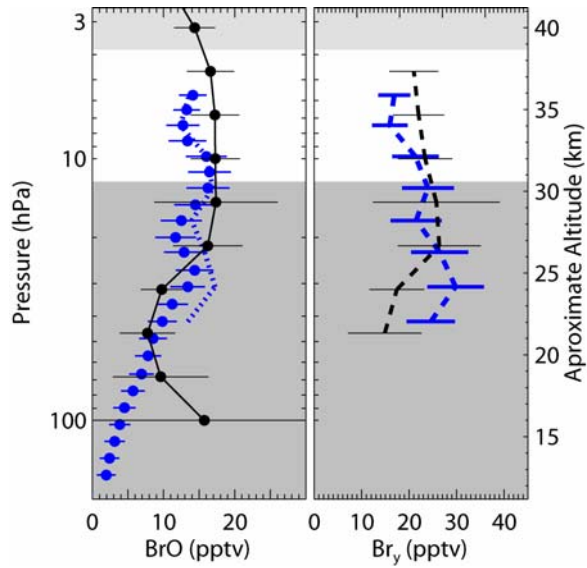
645 Figure 13 Time series of daily zonal mean BrO from 35°N to 45°N for the 10 hPa  
646 pressure surface averaged over the duration of the mission. Version 1.5 is shown in black,  
647 v2.2 in red. Top panel shows nighttime BrO measurements, bottom panel day/night  
648 differences. Error bars are shown for v2.2 but not for v1.5. The discontinuity in v1.5  
649 nighttime data seen when Band 13 was switched off in March 2006 is not seen in v2.2  
650 nighttime data.



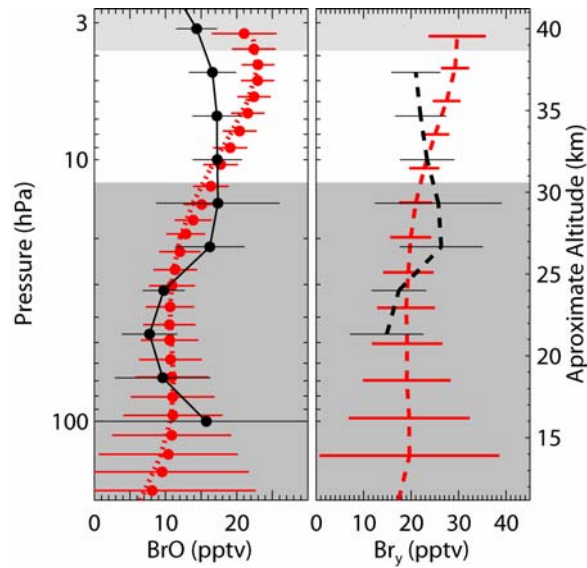
651 Figure 14 Comparison of MLS day/night difference BrO (left-hand panel) and inferred  
 652 Br<sub>y</sub> (right-hand panel) with DOAS data from the March 23, 2003 flight at 68°N. In the  
 653 left-hand panel, the black points show the MLS BrO day/night difference averaged over  
 654 the 149 days of v2.2 data retrieved as of the writing of this manuscript. The MLS BrO  
 655 error bars indicate accuracy. The average solar zenith of the MLS measurements is 40°.  
 656 The non-shaded region indicates where the day/night difference in MLS BrO is  
 657 representative of the daytime BrO. The lightly shaded region indicates where the  
 658 day/night difference in MLS measurements of BrO is not representative of daytime BrO;  
 659 rather, one needs to take account of the non-negligible nighttime BrO, which we have not  
 660 done here. The darker shaded region indicates where MLS measurements of BrO are not  
 661 suitable for scientific use. The green points show DOAS BrO, while the green dotted  
 662 curve shows that data scaled using a photochemical model to a SZA of 65°, the smallest  
 663 SZA attained in March at that latitude. In the right-hand panel, the dashed black curve is  
 664 Br<sub>y</sub> inferred from MLS BrO using a photochemical model. The dashed green curve shows  
 665 Br<sub>y</sub> similarly inferred from DOAS BrO.



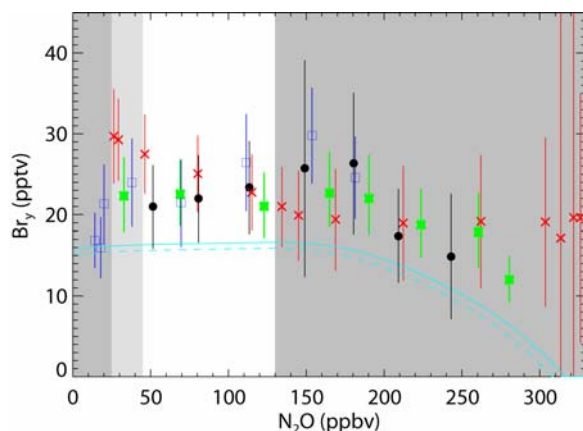
666 Figure 15 Same as Figure 14 except for BrO measurements obtained by the SAOZ-BrO  
667 instrument (blue) on August 24, 2004, at 52°N. The non-shaded region indicates where  
668 the day/night difference in MLS BrO is representative of the daytime BrO. The lightly  
669 shaded region indicates where the day/night difference in MLS measurements of BrO is  
670 not representative of daytime BrO; rather, one needs to take account of the non-negligible  
671 nighttime BrO, which we have not done here. The darker shaded region indicates where  
672 MLS measurements of BrO are not suitable for scientific use.



673 Figure 16 Same as Figure 14 except for BrO measurements obtained by the SLS-2  
674 instrument (red) on September 20, 2005, at 35°N. Error bars on MLS and SLS-2 Br<sub>y</sub> have  
675 been slightly offset for clarity. The non-shaded region indicates where the day/night  
676 difference in MLS BrO is representative of the daytime BrO. The lightly shaded region  
677 indicates where the day/night difference in MLS measurements of BrO is not  
678 representative of daytime BrO; rather, one needs to take account of the non-negligible  
679 nighttime BrO, which we have not done here. The darker shaded region indicates where  
680 MLS measurements of BrO are not suitable for scientific use.



681 Figure 17 Tracer space comparison of Br<sub>y</sub> inferred from measurements of BrO obtained  
682 by MLS and three balloon instruments. The MLS Br<sub>y</sub> (black) is inferred from daily zonal  
683 mean BrO using a photochemical model, and then averaged over latitudes ranging from  
684 55°S to 55°N and over all 149 v2.2 days processed to date. The DOAS (green) Br<sub>y</sub> is  
685 inferred from BrO measured during the March 2003 Kiruna flight, the SAOZ-BrO Br<sub>y</sub>  
686 (blue) is inferred from BrO measured during the August 2004 flight, and the SLS-2  
687 inferred Br<sub>y</sub> (red) is for the September 2005 flight. Also shown is the expected relation  
688 assuming known organic precursors, based on measurements in 1994 [Wamsley *et al.*,  
689 1998] (dashed cyan) and updated to the year of stratospheric entry of 2000 (solid cyan)  
690 [WMO, 2007]. The non-shaded region indicates where the day/night difference in MLS  
691 BrO is representative of the daytime BrO. The lightly shaded region, as well as lower  
692 N<sub>2</sub>O, indicates where the day/night difference in MLS measurements of BrO is not  
693 representative of daytime BrO; rather, one needs to take account of the non-negligible  
694 nighttime BrO. The darker shaded regions indicate where MLS measurements of BrO are  
695 not suitable for scientific use.



## References

- 696  
697  
698 Bedjanian, Y. et al. (2001), Kinetics and mechanism of the OH and OD reactions with  
699 BrO, *Journal of Physical Chemistry A*, 105(25), 6154.
- 700 Chance, K. et al. (1996), Simultaneous measurements of stratospheric HO<sub>x</sub>, NO<sub>x</sub>, and Cl<sub>x</sub>:  
701 Comparison with a photochemical model, *Journal of Geophysical Research-*  
702 *Atmospheres*, 101(D4), 9031.
- 703 Chipperfield, M. (1999), Multiannual simulations with a three-dimensional chemical  
704 transport model, *Journal of Geophysical Research-Atmospheres*, 104(D1), 1781.
- 705 Dorf, M. (2005), Investigation of inorganic stratospheric bromine using balloon-borne  
706 DOAS measurements and model simulations, 203 pp, Ruperto Carola University  
707 of Heidelberg, Heidelberg.
- 708 Dorf, M. et al. (2006a), Balloon-borne stratospheric BrO measurements: comparison with  
709 Envisat/SCIAMACHY BrO limb profiles, *Atmospheric Chemistry and Physics*, 6,  
710 2483.
- 711 Dorf, M. et al. (2006b), Long-term observations of stratospheric bromine reveal slow  
712 down in growth, *Geophysical Research Letters*, 33(24).
- 713 Drouin, B. J. et al. (2001), The rotational spectra, isotopically independent parameters,  
714 and interatomic potentials for the X-1 (2)Pi(3/2) and X-2 (2)Pi(1/2) states of BrO,  
715 *Journal of Molecular Spectroscopy*, 205(1), 128.
- 716 Livesey, N. J., and W. G. Read (2000), Direct retrieval of line-of-sight atmospheric  
717 structure from limb sounding observations, *Geophysical Research Letters*, 27(6),  
718 891.
- 719 Livesey, N. J. et al. (2006a), EOS Microwave Limb Sounder observations of upper  
720 stratospheric BrO: Implications for total bromine, *Geophysical Research Letters*,  
721 33(20).
- 722 Livesey, N. J. et al. (2006b), Retrieval algorithms for the EOS Microwave Limb Sounder  
723 (MLS), *Ieee Transactions on Geoscience and Remote Sensing*, 44(5), 1144.
- 724 Montzka, S. A. et al. (2003), A decline in tropospheric organic bromine, *Geophysical*  
725 *Research Letters*, 30(15).
- 726 Osterman, G. B. et al. (1997), Balloon-borne measurements of stratospheric radicals and  
727 their precursors: Implications for the production and loss of ozone, *Geophysical*  
728 *Research Letters*, 24(9), 1107.
- 729 Pfeilsticker, K. et al. (2000), Lower stratospheric organic and inorganic bromine budget  
730 for the Arctic winter 1998/99, *Geophysical Research Letters*, 27(20), 3305.
- 731 Pundt, I. et al. (2002), Climatology of the stratospheric BrO vertical distribution by  
732 balloon-borne UV-visible spectrometry, *Journal of Geophysical Research-*  
733 *Atmospheres*, 107(D24).
- 734 Read, W. G. et al. (submitted, 2007), Aura Microwave Limb Sounder Upper  
735 Tropospheric and Lower Stratospheric Humidity Validation, *Journal of*  
736 *Geophysical Research-Atmospheres*.
- 737 Rodgers, C. D. (2000), *Inverse Methods for Atmospheric Science, Theory and Practice*,  
738 World Scientific.
- 739 Salawitch, R. J. et al. (2005), Sensitivity of ozone to bromine in the lower stratosphere,  
740 *Geophysical Research Letters*, 32(5).

741 Sander, S. P. et al. (2003), JPL 2002: Chemical Kinetics and Photochemical Data for Use  
742 in Atmospheric Studies, Evaluation No. 14, JPL Publication 02-25, Jet Propulsion  
743 Lab, Pasadena, CA.

744 Sander, S. P. et al. (2006), JPL 2006: Chemical Kinetics and Photochemical Data for Use  
745 in Atmospheric Studies, Evaluation No. 15, JPL Publication 06-2, Jet Propulsion  
746 Lab, Pasadena, CA.

747 Santee, M. L. et al. (2007), Validation of the Aura Microwave Limb Sounder ClO  
748 measurements, *Journal of Geophysical Research-Atmospheres*.

749 Sioris, C. E. et al. (2006), Latitudinal and vertical distribution of bromine monoxide in  
750 the lower stratosphere from Scanning Imaging Absorption Spectrometer for  
751 Atmospheric Chartography limb scattering measurements, *Journal of Geophysical  
752 Research-Atmospheres*, 111(D14).

753 Soller, R. et al. (2001), Temperature-dependent rate coefficients for the reactions of Br(P-  
754 2(3/2)), Cl(P-2(3/2)), and O(P-3(J)) with BrONO<sub>2</sub>, *Journal of Physical Chemistry  
755 A*, 105(9), 1416.

756 Stachnik, R. A. et al. (1992), Submillimeter Wave Heterodyne Measurements of  
757 Stratospheric ClO, HCl, O<sub>3</sub>, and HO<sub>2</sub> - 1st Results, *Geophysical Research  
758 Letters*, 19, 1931.

759 Wamsley, P. R. et al. (1998), Distribution of halon-1211 in the upper troposphere and  
760 lower stratosphere and the 1994 total bromine budget, *Journal of Geophysical  
761 Research-Atmospheres*, 103(D1), 1513.

762 Waters, J. W. et al. (2006), The Earth Observing System Microwave Limb Sounder (EOS  
763 MLS) on the Aura satellite, *Ieee Transactions on Geoscience and Remote  
764 Sensing*, 44(5), 1075.

765 WMO (2003), World Meteorological Organization, Global ozone research and  
766 monitoring project, Report No. 47, Scientific assessment of ozone depletion:  
767 2002, Geneva, Switzerland.

768 WMO (2007), World Meteorological Organization, Global ozone research and  
769 monitoring project, Report No. 50, Scientific assessment of ozone depletion:  
770 2006, Geneva, Switzerland.

771 Yamada, M. M. et al. (2003), Submillimeter-wave measurements of the pressure  
772 broadening of BrO, *Journal of Quantitative Spectroscopy & Radiative Transfer*,  
773 82(1-4), 391.

774  
775